Davis-Chandrasekhar-Fermi method employed with Ground-state-Alignment

Measurement of magnetic field strength in the ISM

Parth Pavaskar, Prof. Huirong Yan, Prof. Jungyeon Cho

Theoretische Astro-Teilchen (THAT) Physik, DESY

Plasma Astrophysics Group, Universität Potsdam

Obertrubach, 07.10.2022

HELMHOLTZ

Magnetic fields in the ISM

Why bother?

Magnetic fields in the ISM

Why bother?

Magnetic fields govern the plasma dynamics in the ISM,

Magnetic fields in the ISM

Why bother?

Magnetic fields govern the plasma dynamics in the ISM, and are relevant in processes like:

- Plasma turbulence
- Molecular cloud collapse / star formation
- CR transport and acceleration
- Accretion disk dynamics
- Jet propagation
- Solar wind heating
- Chemical evolution

Magnetic fields in the ISM

Why bother?

Magnetic fields govern the plasma dynamics in the ISM, and are relevant in processes like:

- Plasma turbulence
- Molecular cloud collapse / star formation
- CR transport and acceleration
- Accretion disk dynamics
- Jet propagation
- Solar wind heating
- Chemical evolution

Field strength measurements are non-trivial and rely solely on (spectro-) polarimetry observations.

Magnetic fields in the ISM

Why bother?

Magnetic fields govern the plasma dynamics in the ISM, and are relevant in processes like:

- Plasma turbulence
- Molecular cloud collapse / star formation
- CR transport and acceleration
- Accretion disk dynamics
- Jet propagation
- Solar wind heating
- Chemical evolution

Field strength measurements are non-trivial and rely solely on (spectro-) polarimetry observations. Dust grain alignment is most commonly used.

Movitation

The problem with dust

Movitation

The problem with dust

The dust polarization method is based on the the theory of localized dust grain alignment due to the turbulent magnetic field.

Movitation

The problem with dust

The dust polarization method is based on the the theory of localized dust grain alignment due to the turbulent magnetic field

- Sizes and shapes of individual grains varies significantly
- Different chemical compositions
- Polarization observations are obtained from averaged visible/IR continuum

Movitation

The problem with dust

The dust polarization method is based on the the theory of localized dust grain alignment due to the turbulent magnetic field

- Sizes and shapes of individual grains varies significantly
- Different chemical compositions
- Polarization observations are obtained from averaged visible/IR continuum

Important

The Davis-Chandrasekhar-Fermi technique

The classical DCF method

- Proposed independently by Davis (1951) and Chandrasekhar & Fermi (1953).

The Davis-Chandrasekhar-Fermi technique

The classical DCF method

- Proposed independently by Davis (1951) and Chandrasekhar & Fermi (1953).

$$B_{0,\mathrm{pos}} = \xi\sqrt{4\pi\bar{\rho}}\,\frac{\delta v_{\mathrm{los}}}{\delta\phi}$$

The Davis-Chandrasekhar-Fermi technique

The classical DCF method

- Proposed independently by Davis (1951) and Chandrasekhar & Fermi (1953).

$$B_{0,\mathrm{pos}} = \xi \sqrt{4\pi\bar{\rho}}\, \frac{\delta \mathrm{v}_{\mathrm{los}}}{\delta\phi}$$

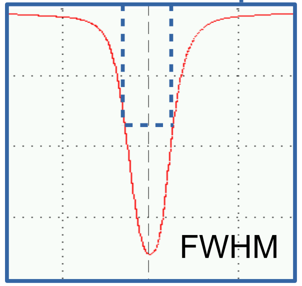

The Davis-Chandrasekhar-Fermi technique

The classical DCF method

- Proposed independently by Davis (1951) and Chandrasekhar & Fermi (1953).

$$B_{0,\mathrm{pos}} = \xi \sqrt{4\pi\bar{\rho}} \frac{\delta v_{\mathrm{los}}}{\delta\phi}$$

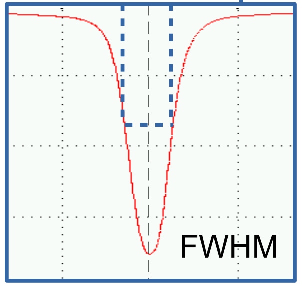

$$\phi_P = \frac{1}{2}\tan^{-1}\frac{U}{Q}$$

The Davis-Chandrasekhar-Fermi technique

The classical DCF method

- Proposed independently by Davis (1951) and Chandrasekhar & Fermi (1953).

$$B_{0,\mathrm{pos}} = \xi \sqrt{4\pi\bar{\rho}}\, \frac{\delta v_{\mathrm{los}}}{\delta\phi}$$

$\sim 0.4 - 0.6$

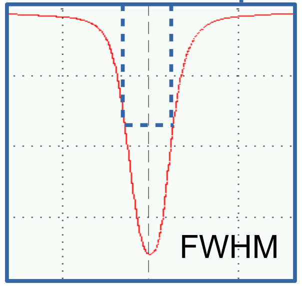

$$\phi_P = \frac{1}{2}\tan^{-1}\frac{U}{Q}$$

The Davis-Chandrasekhar-Fermi technique

The classical DCF method

- Proposed independently by Davis (1951) and Chandrasekhar & Fermi (1953).
- Underlying assumptions:
  - turbulence is purely Alfvénic,
  - the rms velocity and magnetic field fluctuations are isotropic,
  - the angle between the POS projected turbulent and mean magnetic field is small, and
  - the turbulent field is much weaker than the mean field

$$B_{0,\mathrm{pos}} = \xi \sqrt{4\pi\bar{\rho}} \frac{\delta v_{\mathrm{los}}}{\delta\phi}$$

$\sim 0.4 - 0.6$

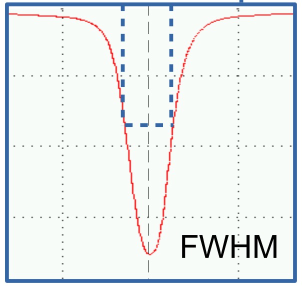

$$\phi_P = \frac{1}{2}\tan^{-1}\frac{U}{Q}$$

The Davis-Chandrasekhar-Fermi technique

The modified DCF method (Cho & Yoo 2016)

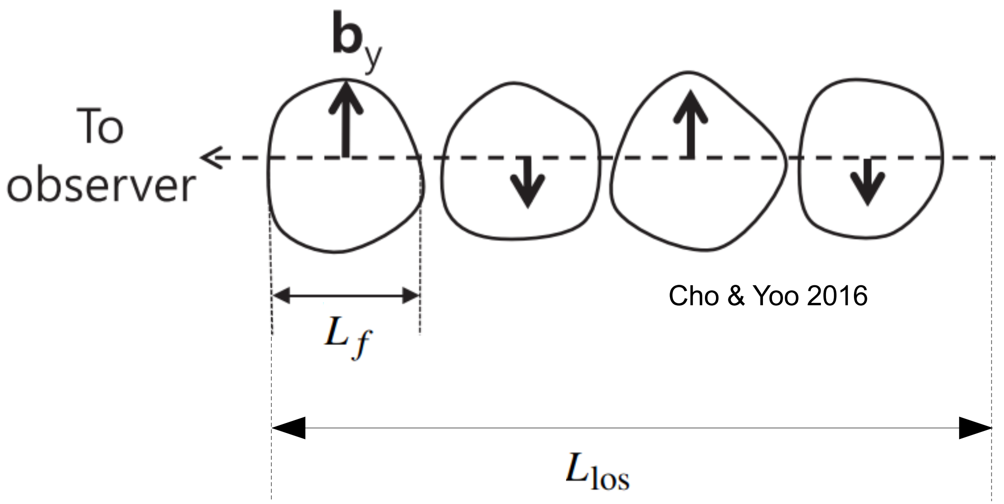

L_f - turbulence driving scale

$L_{\rm los}$ - LOS depth

The Davis-Chandrasekhar-Fermi technique

The modified DCF method (Cho & Yoo 2016)

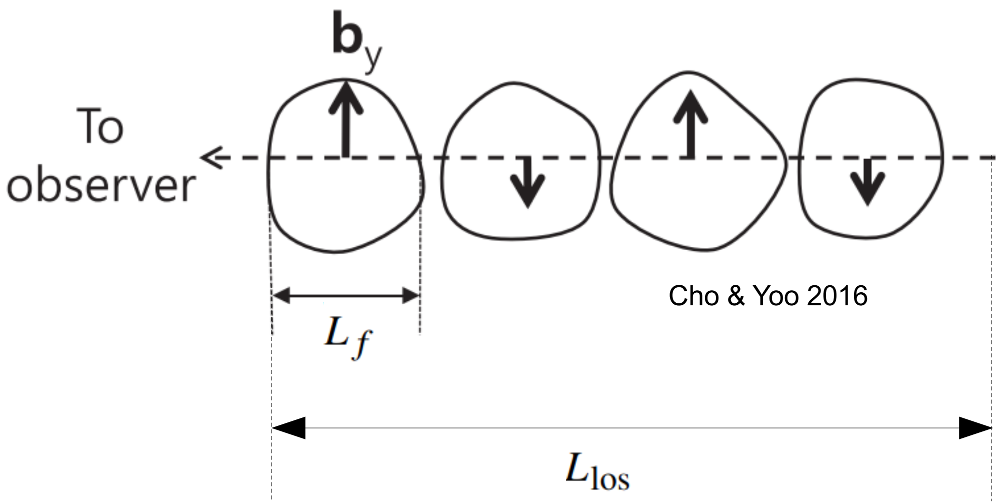

Cho & Yoo 2016

L_f - turbulence driving scale

L_{los} - LOS depth

$$\delta\phi \sim \frac{\delta \mathrm{b}_{\perp,\text{pos}}}{B_{0,\text{pos}}} \sqrt{L_f / L_{\text{los}}}$$

The Davis-Chandrasekhar-Fermi technique

The modified DCF method (Cho & Yoo 2016)

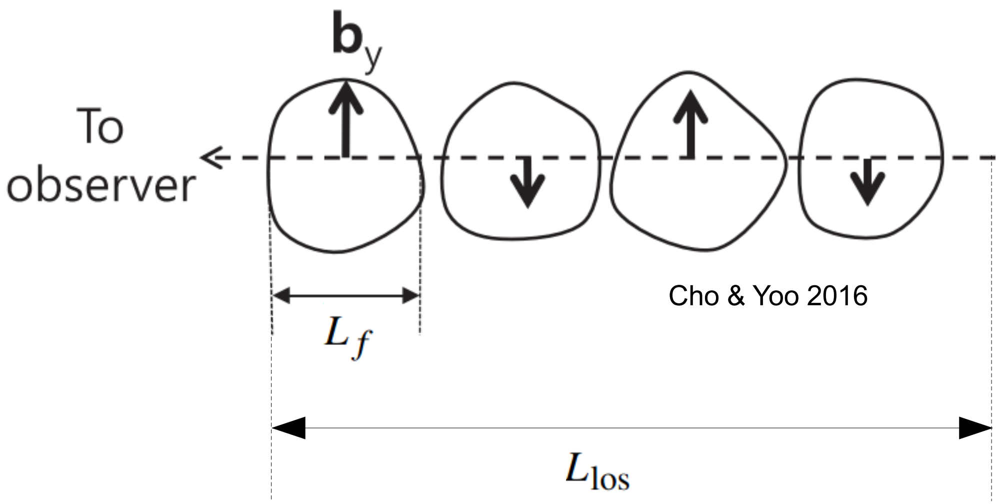

L_f - turbulence driving scale

L_{los} - LOS depth

$$\delta\phi \sim \frac{\delta b_{\perp,pos}}{B_{0,pos}} \sqrt{L_f / L_{los}}$$

The classical method does not consider the effects of the driving scale of turbulence

The Davis-Chandrasekhar-Fermi technique

The modified DCF method (Cho & Yoo 2016)

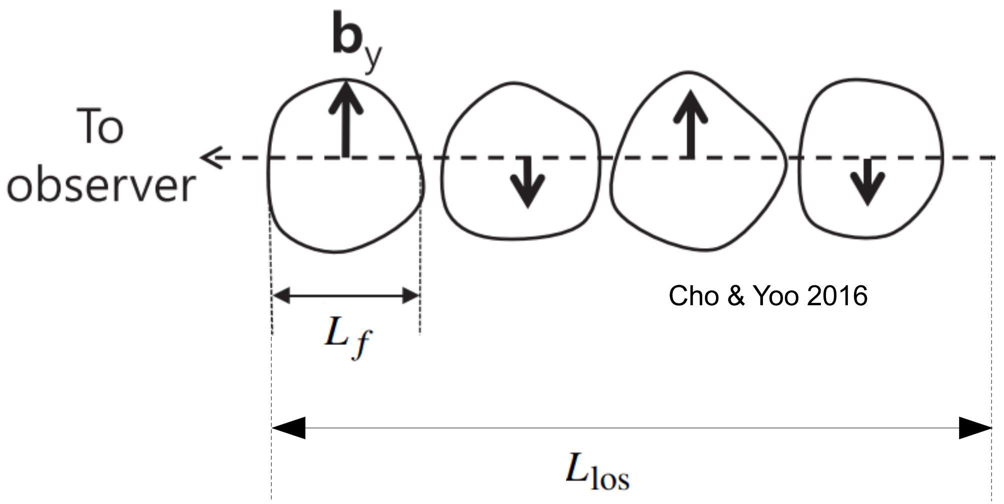

L_f - turbulence driving scale

$L_{\rm los}$ - LOS depth

$$\delta\phi \sim \frac{\delta b_{\perp,\rm pos}}{B_{0,\rm pos}} \sqrt{L_f / L_{\rm los}}$$

The classical method does not consider the effects of the driving scale of turbulence

Modified DCF method:

$$B_{0,\rm pos} = \xi' \sqrt{4\pi\bar{\rho}} \frac{\delta V_c}{\delta\phi}$$

The Davis-Chandrasekhar-Fermi technique

The modified DCF method (Cho & Yoo 2016)

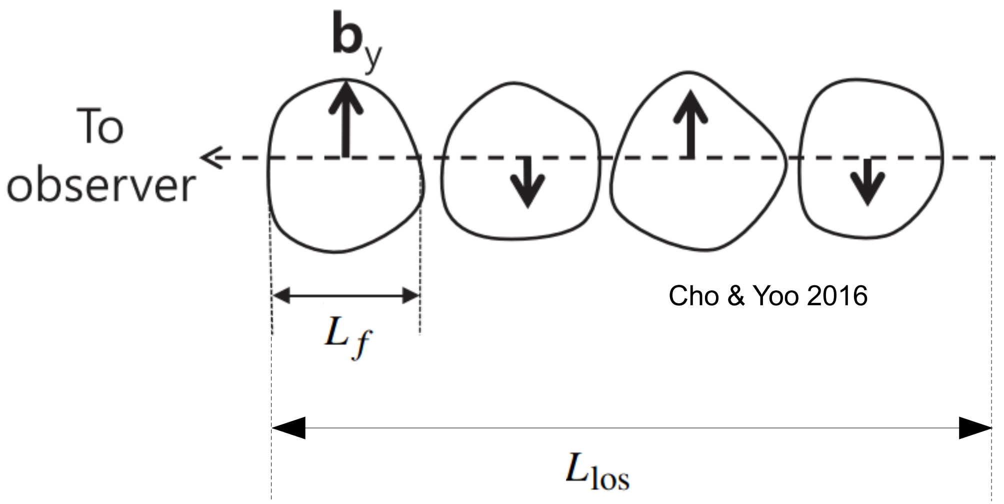

L_f - turbulence driving scale

$L_{\rm los}$ - LOS depth

$$\delta\phi \sim \frac{\delta b_{\perp,\rm pos}}{B_{0,\rm pos}} \sqrt{L_f / L_{\rm los}}$$

The classical method does not consider the effects of the driving scale of turbulence

Modified DCF method:

$$B_{0,\rm pos} = \xi' \sqrt{4\pi\bar{\rho}}\, \frac{\delta V_c}{\delta\phi}$$

$$V_{c,i} = \int v_{\rm los}\, I_i(v_{\rm los})\, dv_{\rm los} \Big/ \int I_i(v_{\rm los})\, dv_{\rm los}$$

The Davis-Chandrasekhar-Fermi technique

The modified DCF method (Cho & Yoo 2016)

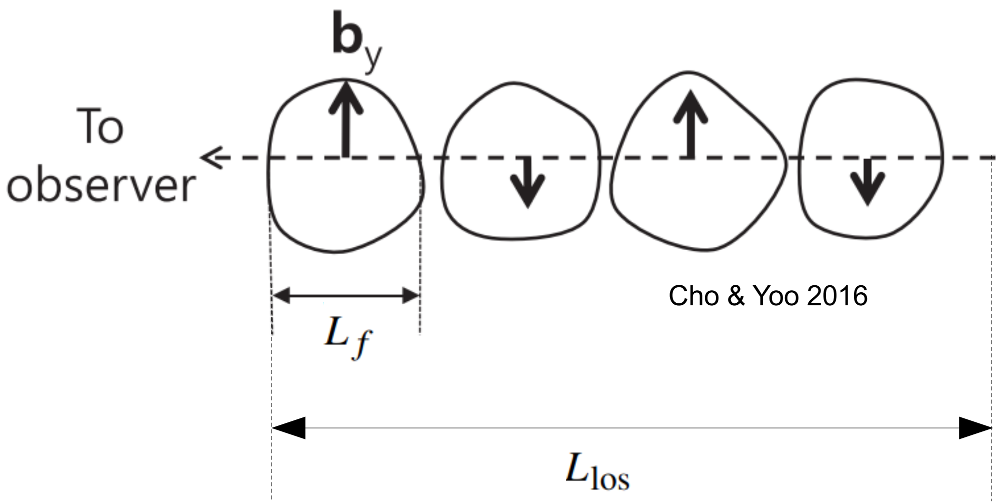

L_f - turbulence driving scale

$L_{\rm los}$ - LOS depth

$$\delta\phi \sim \frac{\delta b_{\perp,\rm pos}}{B_{0,\rm pos}} \sqrt{L_f / L_{\rm los}}$$

The classical method does not consider the effects of the driving scale of turbulence

Modified DCF method:

$$B_{0,\rm pos} = \xi' \sqrt{4\pi\bar{\rho}} \frac{\delta V_c}{\delta\phi}$$

$$V_{\rm c,i} = \int v_{\rm los} I_i(v_{\rm los})\, dv_{\rm los} \Big/ \int I_i(v_{\rm los})\, dv_{\rm los}$$

$\xi' \sim 0.7 - 1.0$

Ang. momentum

Ground-state-Alignment

Polarization of spectral lines

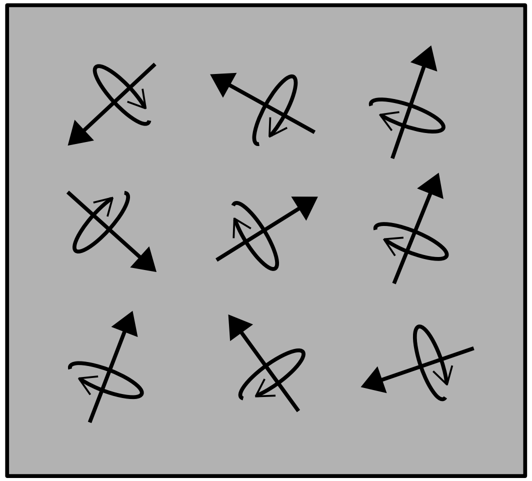

Ground-state-Alignment

Polarization of spectral lines

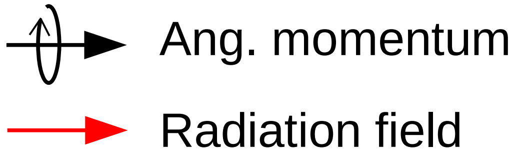

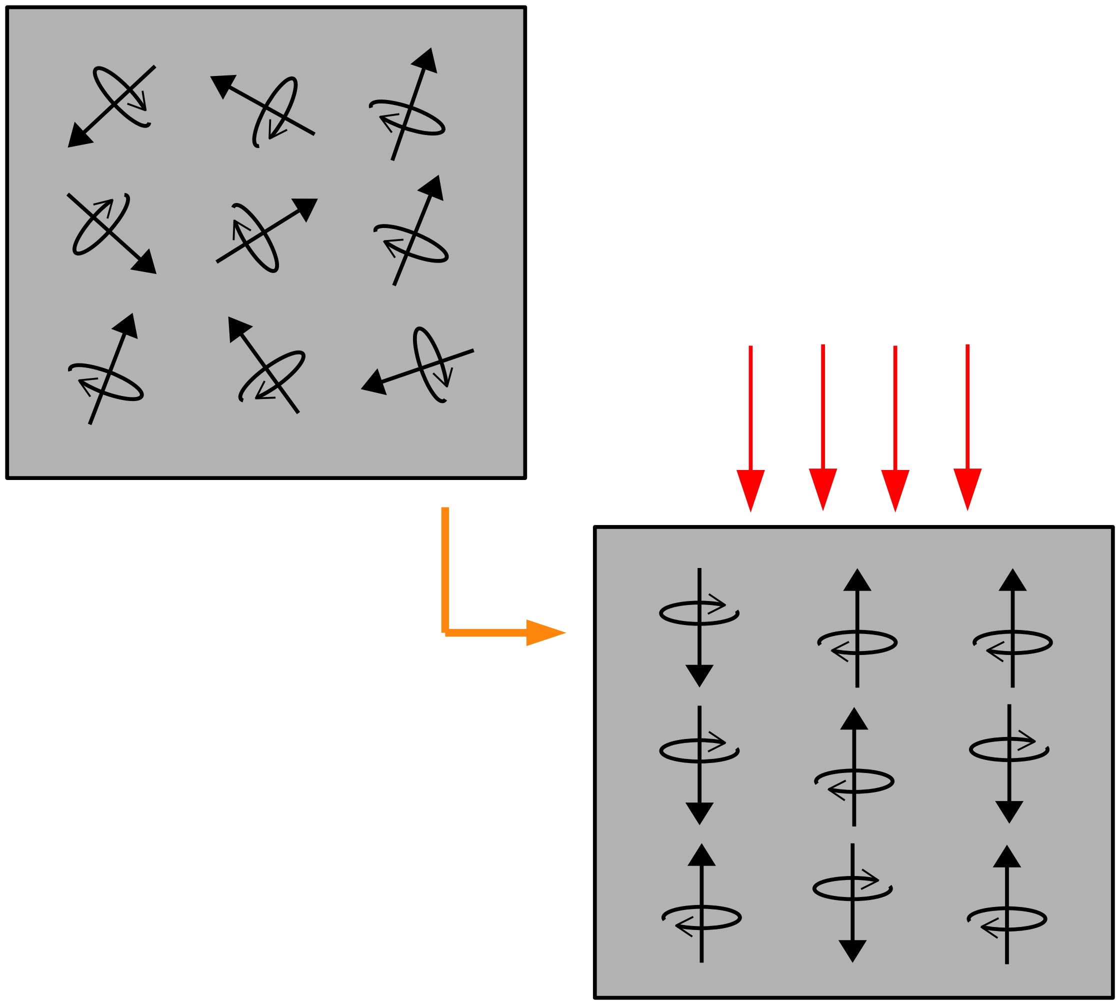

Ground-state-Alignment

Polarization of spectral lines

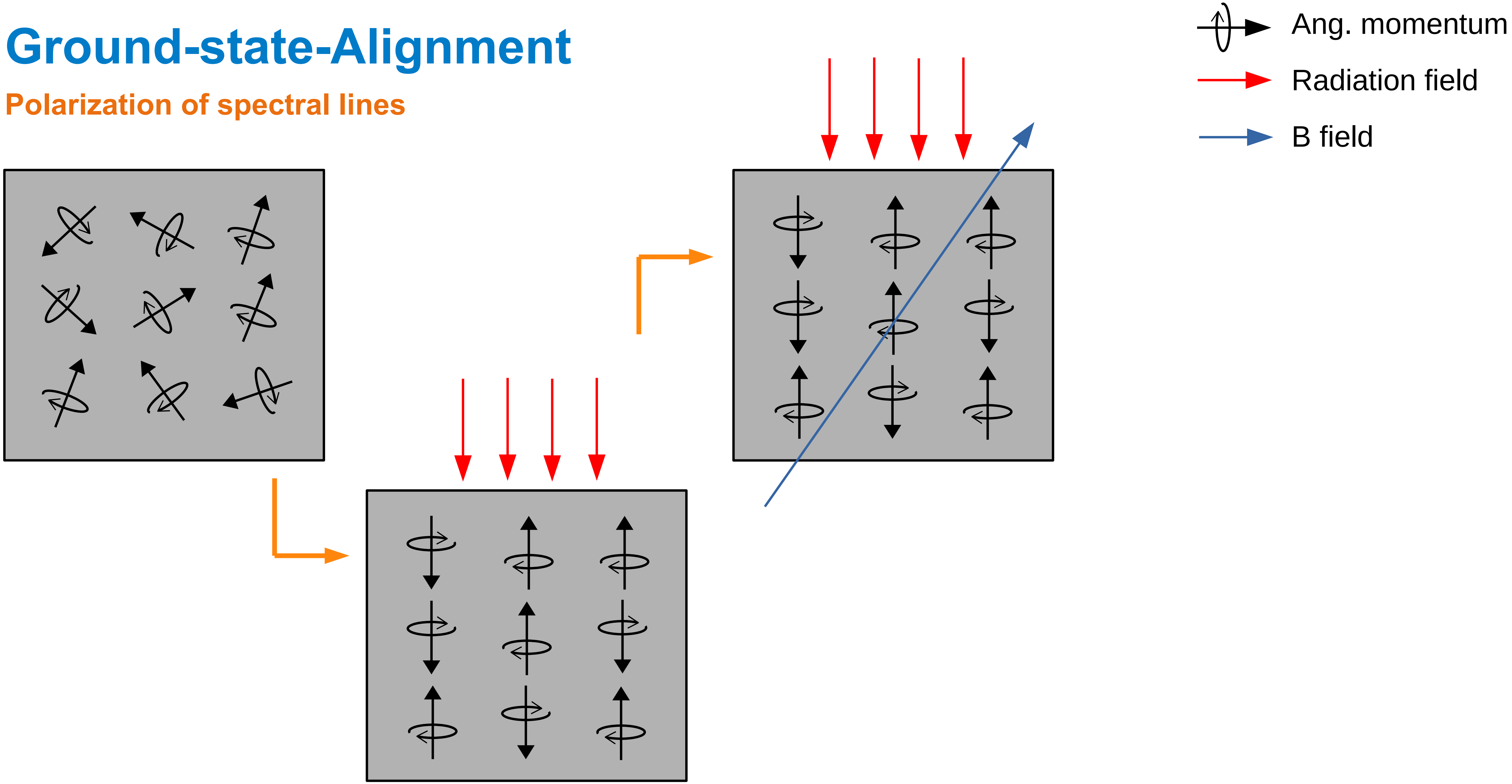

Ground-state-Alignment

Polarization of spectral lines

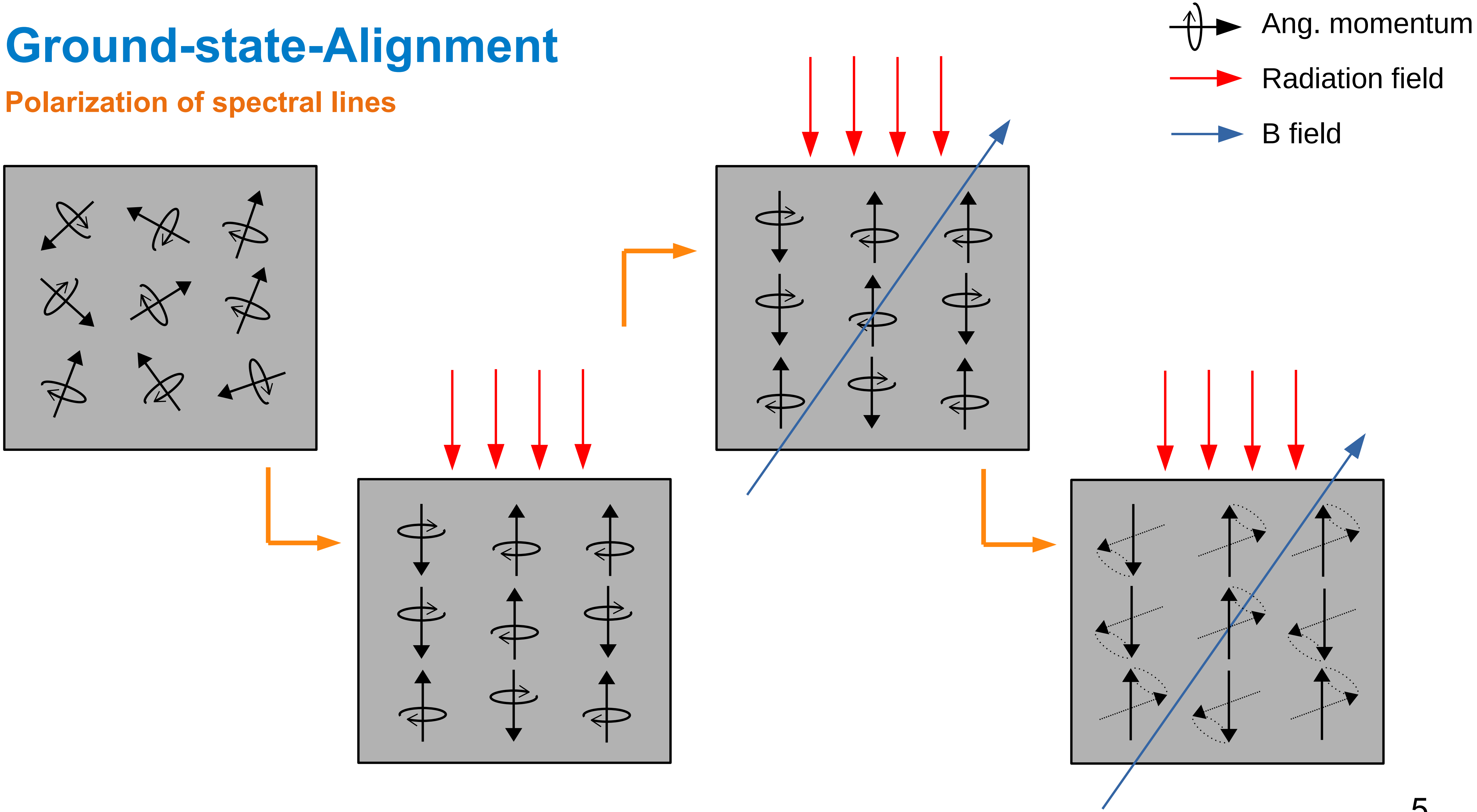

Ground-state-Alignment

Polarization of spectral lines

Ground-state-Alignment refers to the differential occupation of sublevels of the ground state.

Ground-state-Alignment

Polarization of spectral lines

Ground-state-Alignment refers to the differential occupation of sublevels of the ground state.

- Conditions for GSA effect:
  - Anisotropic radiation
  - Fine (or hyperfine) structure in the ground state
  - Radiative dominant regime
  - Long lived ground (or metastable) state

Ground-state-Alignment

Polarization of spectral lines

Ground-state-Alignment refers to the differential occupation of sublevels of the ground state.

- Conditions for GSA effect:
  - Anisotropic radiation
  - Fine (or hyperfine) structure in the ground state
  - Radiative dominant regime
  - Long lived ground (or metastable) state

$$\nu_{\mathrm{L}} > R_F > \tau_c^{-1}$$

Ground-state-Alignment

Polarization of spectral lines

Ground-state-Alignment refers to the differential occupation of sublevels of the ground state.

- Conditions for GSA effect:
  - Anisotropic radiation
  - Fine (or hyperfine) structure in the ground state
  - Radiative dominant regime
  - Long lived ground (or metastable) state

$$\nu_{\mathrm{L}} > R_F > \tau_c^{-1}$$

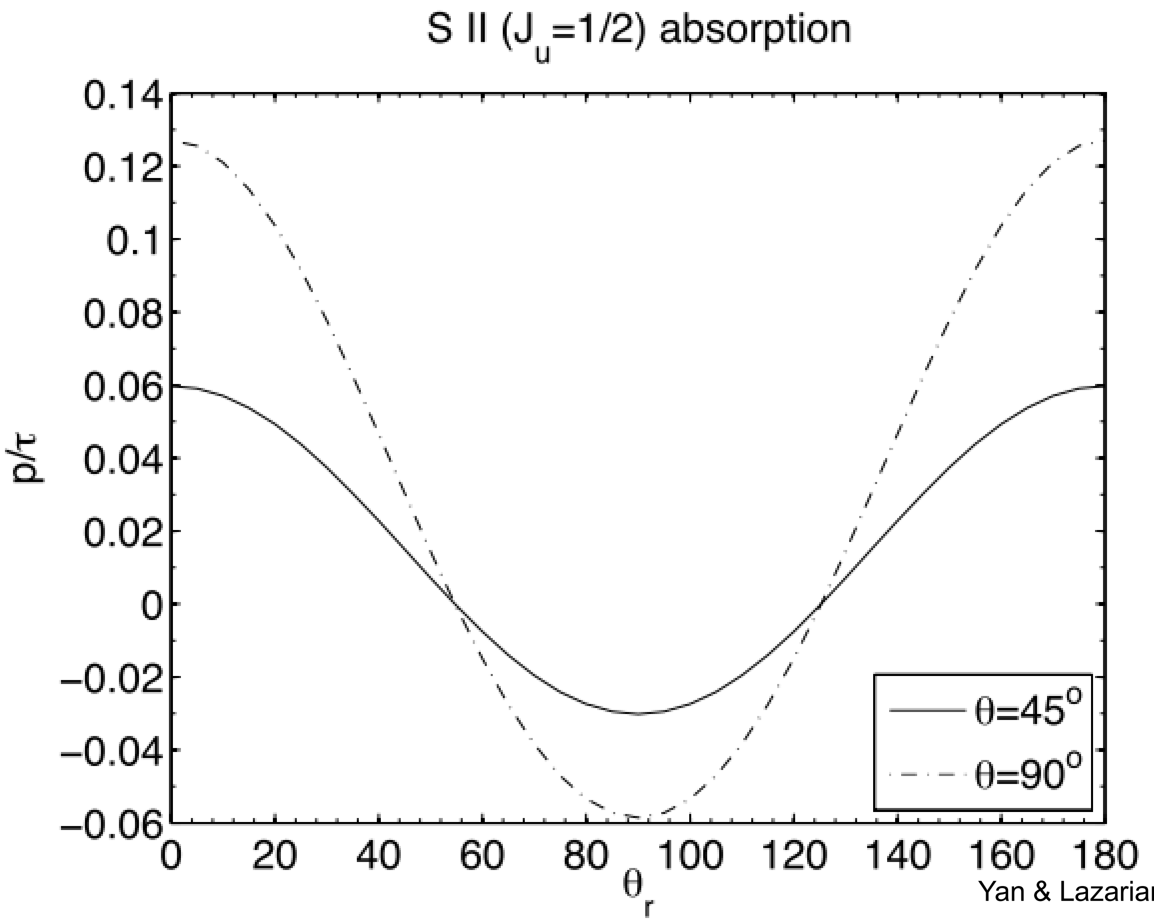

Yan & Lazarian 2006

$$P = \frac{1.5\,\sigma_0^2(J_1,\theta_r)\,\sin^2\theta_B\,\omega^2_{J_1J_2}}{\sqrt{2} + \sigma_0^2(J_1,\theta_r)\,(1-1.5\sin^2\theta_B)\,\omega^2_{J_1J_2}}$$

$$\sigma_0^2 \equiv \rho_0^2/\rho_0^0\ , \quad \omega^2_{J_1J_u} \equiv \{1,1,2;J_1,J_1,J_u\}/\{1,1,0;J_1,J_1,J_u\}$$

A numerical study

Simulation setup

- Basic setup – step 1
  - 3D ideal MHD simulation with a finite-difference scheme (PENCIL)
  - External magnetic field along box-X axis
  - Anisotropic box-parallel radiation field from an O-type-like star placed along X axis
  - Ornstein-Uhlenbeck process to force turbulence solenoidally with specific driving wavenumber
  - Line-of-sight is fixed along the Z direction

A numerical study

Simulation setup

- Basic setup – step 1
  - 3D ideal MHD simulation with a finite-difference scheme (PENCIL)
  - External magnetic field along box-X axis
  - Anisotropic box-parallel radiation field from an O-type-like star placed along X axis
  - Ornstein-Uhlenbeck process to force turbulence solenoidally with specific driving wavenumber
  - Line-of-sight is fixed along the Z direction

- Expanding the parameter range – step 2
  - Repeat simulations for varying Alfvén mach numbers (sub-Alfvénic to trans-Alfvénic)
  - Rotate the sim. box so the B_0 scans the full solid angle
  - Change the radiation field inclination angle in the XZ plane

A numerical study

Simulation setup

- Basic setup – step 1
  - 3D ideal MHD simulation with a finite-difference scheme (PENCIL)
  - External magnetic field along box-X axis
  - Anisotropic box-parallel radiation field from an O-type-like star placed along X axis
  - Ornstein-Uhlenbeck process to force turbulence solenoidally with specific driving wavenumber
  - Line-of-sight is fixed along the Z direction

- Expanding the parameter range – step 2
  - Repeat simulations for varying Alfvén mach numbers (sub-Alfvénic to trans-Alfvénic)
  - Rotate the sim. box so the B_0 scans the full solid angle
  - Change the radiation field inclination angle in the XZ plane

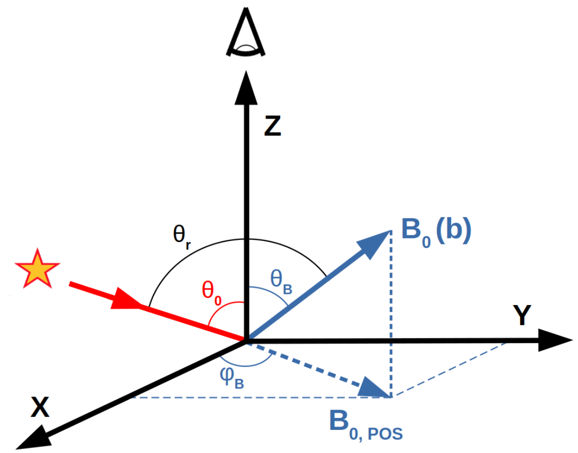

A numerical study

- Synthetic observations – step 3
  - Calculate linear Stokes vector at each grid for the [C II] λ157 μm fine structure emission line
  - Intensity (density) weighted LOS integration to obtain synthetic polarization maps
  - DCF analysis using pol. maps and line widths
  - Repeat over entire parameter range

A numerical study

- Synthetic observations – step 3
  - Generate linear Stokes vector at each grid for the [C II] λ157 μm fine structure emission line
  - Intensity (density) weighted LOS integration to obtain synthetic polarization maps
  - DCF analysis using pol. maps and line widths
  - Repeat over entire parameter range

Name	Resolution	Alfvén velocity (v_A)	Alfvén Mach number (M_A)	Sonic Mach number (M_s)	Driving wavenumber (k_f)	$B_{0,\mathrm{pos}}$
d_017	512^3	0.17	1.10	1.87	2	0.94
d_024	512^3	0.24	0.70	1.68	2	1.00
d_030	512^3	0.30	0.66	1.98	2	1.17
d_040	512^3	0.40	0.50	2.00	2	1.16
d_050	512^3	0.50	0.40	2.00	2	1.32
d_060	512^3	0.60	0.33	1.98	2	1.23
d_070	512^3	0.70	0.26	1.82	2	1.30
k_024	512^3	0.12	0.50	2.50	10	1.31

Pavaskar et al. 2022

A numerical study

Sample results

Pavaskar et al. 2022

- Sample results from 3 different data-cubes
- Radiation field direction is fixed along x-axis ($\theta_0 = 90^o$)

Mean B-field

Radiation field

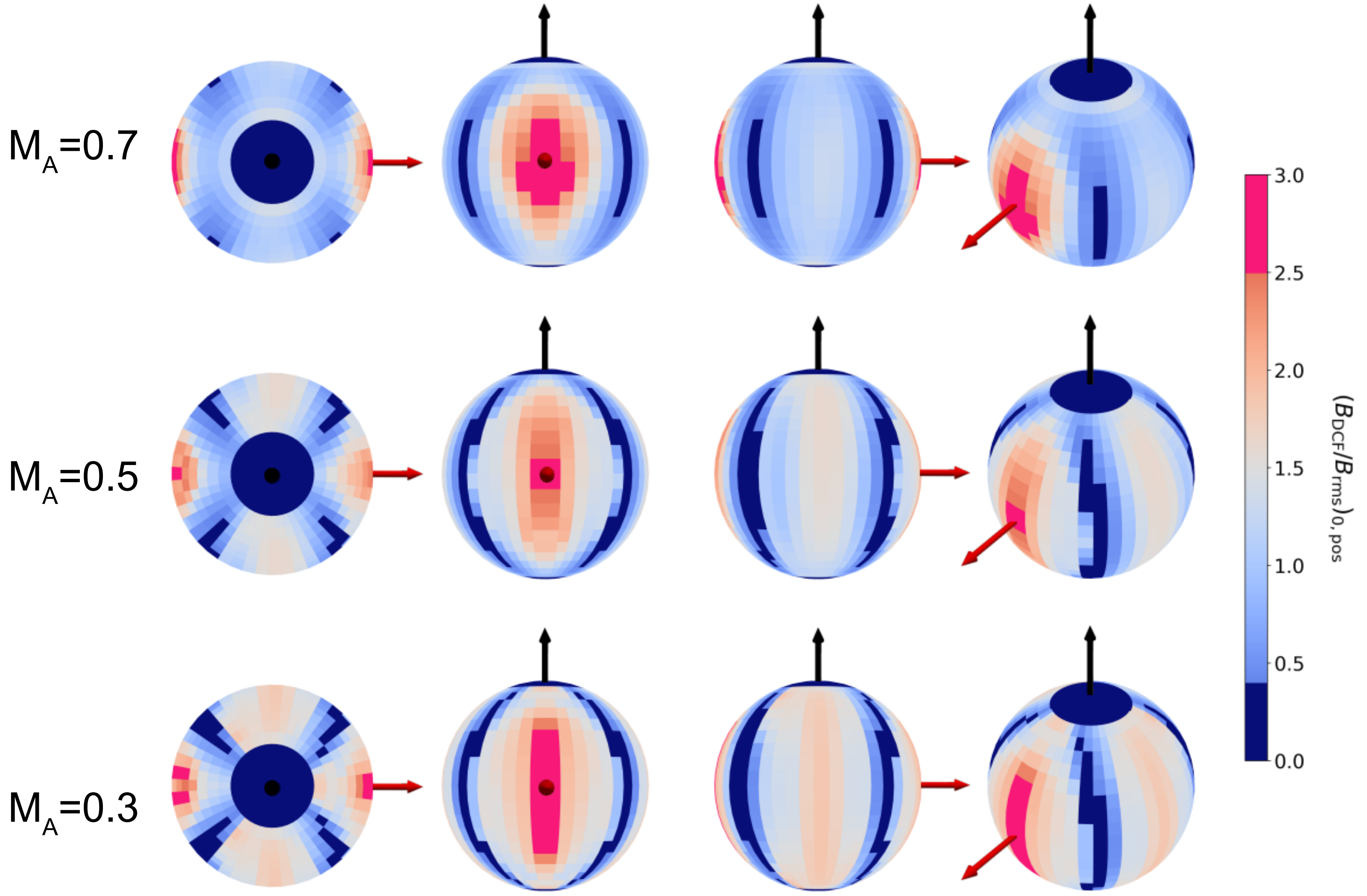

Take-home message

Take-home message

It works!

Take-home message

It works!

- DCF technique can be employed with polarization from GSA effect.
- It is possible to observe polarization and velocity dispersion signatures from the same spectral lines.
- The method is readily applicable on valid transition lines from archival polarimetry data.

Take-home message

It works!

- DCF technique can be employed with polarization from GSA effect.
- It is possible to observe polarization and velocity dispersion signatures from the same spectral lines.
- The method is readily applicable on valid transition lines from archival polarimetry data.

◆ Pavaskar et al. 2022, MNRAS

Take-home message

It works!

- DCF technique can be employed with polarization from GSA effect.
- It is possible to observe polarization and velocity dispersion signatures from the same spectral lines.
- The method is readily applicable on valid transition lines from archival polarimetry data.

◆ Pavaskar et al. 2022, MNRAS

Further work to be done

- A better filter to break the Van-Vleck degeneracy.
- 3D tomography of ISM magnetic fields in PPV space using thin velocity-slice analysis.

Thank you

Contact

Deutsches Elektronen-
Synchrotron DESY

www.desy.de

Parth Pavaskar
Deutsches Elektronen-Synchrotron Zeuthen
Institut für Physik und Astronomie, Universität Potsdam

parth.pavaskar@desy.de

Extra slides

GSA regime according to magnetic field strength

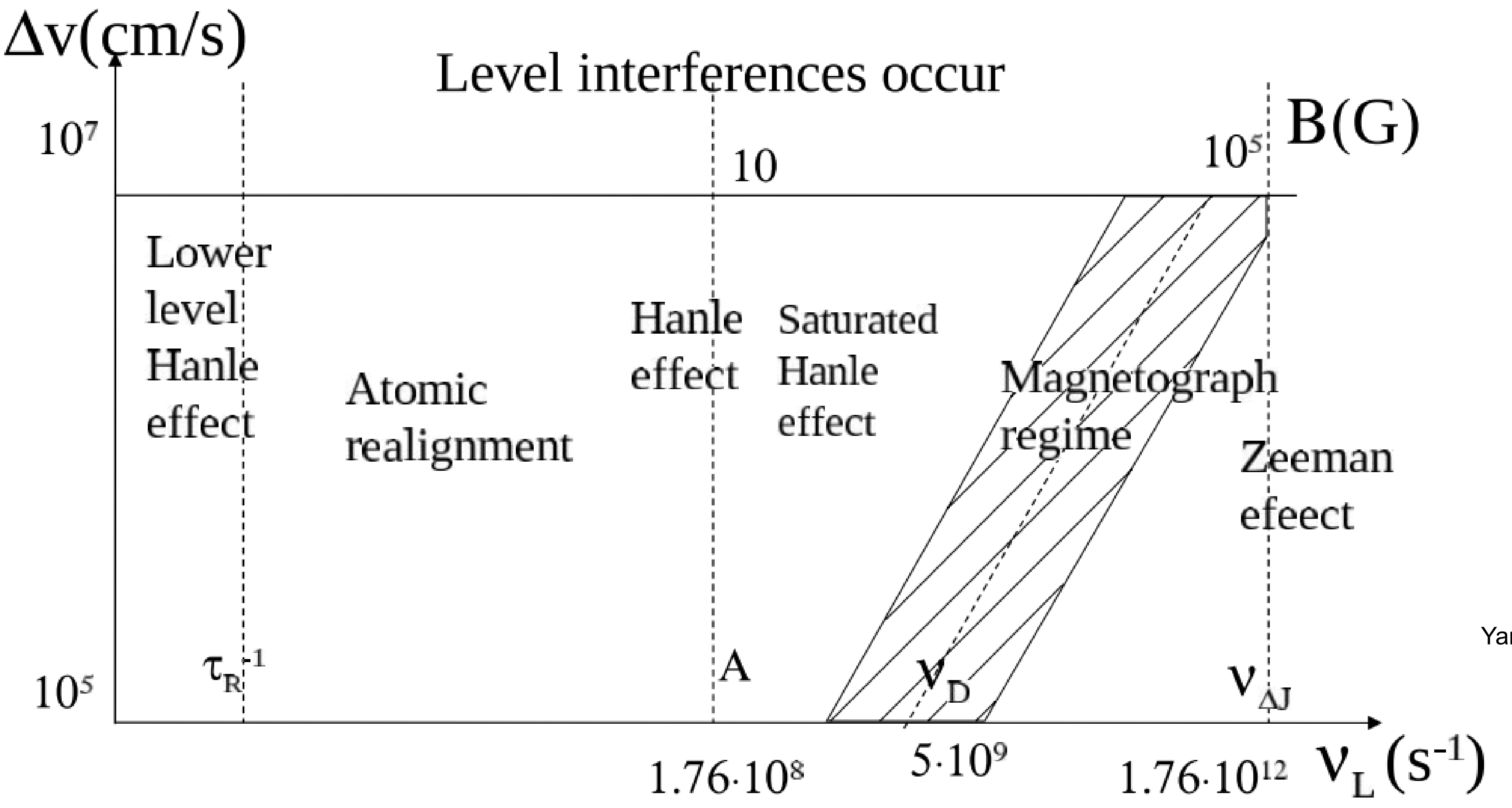

Yan & Lazarian 2008

Extra slides

Emission and absorption lines and their theoretical max. polarization according to GSA

Calculated for ISRF

Emission Lines

Species	Lower State	Upper State	Wavelength (Å)	$\lvert P_{max} \rvert$ (%)
S II	$4S^o_{3/2}$	$4P_{3/2}$	1253.81	30.6
		$4P_{5/2}$	1259.52	31.4
O I	$3P_0$	$3S^o$	1306	16
	$3P_1$	$3S^o$	1304	8.5
	$3P_2$	$3S^o$	1302	1.7
	$3P$	$3S^o$	5555, 6046, 7254	2.3
	$3P_0$	$3D^o$	1028	4.29
	$3P_1$	$3D^o$	1027	7.7
	$3P_2$	$3D^o$	1025	10.6
	$3P$	$3D^o$	5513, 5958, 7002	1.3

Absorption Lines

Species	Ground State	Excited State	Wavelength (Å)	P_{max} (%)
Ti II	$a4F_{3/2}$	$z4G^o_{5/2}$	3384.74	−0.7
		$z4F^o_{5/2}$	3230.13	−0.7
		$z4F^o_{3/2}$	3242.93	2.9
		$z4D^o_{3/2}$	3067.25	2.9
		$z4D^o_{1/2}$	3073.88	7.3

Yan & Lazarian 2012

Extra slides

Sub-mm emission and absorption lines and their theoretical max. polarization according to GSA Calculated for SFR

Table 1. Maximum polarisation for submillimetre emission lines.

Species	Transition	Wavelength	max(P)
[C I]	$3P_1 \rightarrow 3P_0$	610 μm	21 per cent[a]
[C I]	$3P_2 \rightarrow 3P_1$	370 μm	18 per cent[b]
[C II]	$2P^{\circ}_{3/2} \rightarrow 2P^{\circ}_{1/2}$	157.7 μm	28.5 per cent[a]
[O I]	$3P_1 \rightarrow 3P_2$	63.2 μm	4.2 per cent[a]
[Si I]	$3P_1 \rightarrow 3P_0$	129.7 μm	20 per cent[a]
[Si I]	$3P_2 \rightarrow 3P_1$	68.5 μm	18 per cent[b]
[Si II]	$2P^{\circ}_{3/2} \rightarrow 2P^{\circ}_{1/2}$	34.8 μm	12.6 per cent[b]
[S I]	$3P_1 \rightarrow 3P_2$	25.2 μm	3.2 per cent[a]
[Fe II]	$a6D_{7/2} \rightarrow a6D_{9/2}$	26.0 μm	4.9 per cent[a]

Table 2. Maximum polarisation for submillimetre absorption lines.

Species	Transition	Wavelength	$\max(P/\tau)$
[C I]	$3P_1 \rightarrow 3P_2$	370 μm	2 per cent[a]
[O I]	$3P_2 \rightarrow 3P_1$	63.2 μm	30.8 per cent[b]
[O I]	$3P_1 \rightarrow 3P_0$	145.5 μm	49.1 per cent[c]
[S I]	$3P_2 \rightarrow 3P_1$	25.2 μm	30.1 per cent[d]
[S I]	$3P_1 \rightarrow 3P_0$	56.3 μm	45.2 per cent[e]
[Si I]	$3P_1 \rightarrow 3P_2$	370 μm	2 per cent[a]
[Fe II]	$a6D_{9/2} \rightarrow a6D_{7/2}$	26.0 μm	9.9 per cent[f]

Zhang & Yan 2018

Extra slides

The DCF method bones

Proposed to measure the mean magnetic field strength based on the theory of Alfvénic turbulence.

$$\delta \mathrm{v} \sim \frac{\delta \mathrm{b}}{\sqrt{4\pi\bar{\rho}}}$$

$$B_{0,\mathrm{pos}} \sim \sqrt{4\pi\bar{\rho}}\,\frac{\delta \mathrm{v}}{\delta b / B_{0,\mathrm{pos}}}$$

Such that :

- The rms velocity and magnetic field fluctuations are isotropic and

$$\delta \mathrm{b} \sim \delta \mathrm{b}_{\perp,\mathrm{pos}}\,, \quad \delta \mathrm{v} \sim \delta \mathrm{v}_{\mathrm{los}}$$

- The angle between the POS projected turbulent and mean magnetic field is small,

$$\frac{\delta \mathrm{b}_{\perp,\mathrm{los}}}{B_{0,\mathrm{pos}}} \sim \tan(\delta\phi) \sim \delta\phi$$

- The turbulent field is much weaker than the mean field

we get the field strength in terms of observables

$$B_{0,\mathrm{pos}} = \xi \sqrt{4\pi\bar{\rho}}\,\frac{\delta \mathrm{v}_{\mathrm{los}}}{\delta\phi}$$

Extra slides

Driving scale discrepancy in DCF

However, the classical method does not consider the effects of the driving scale of turbulence

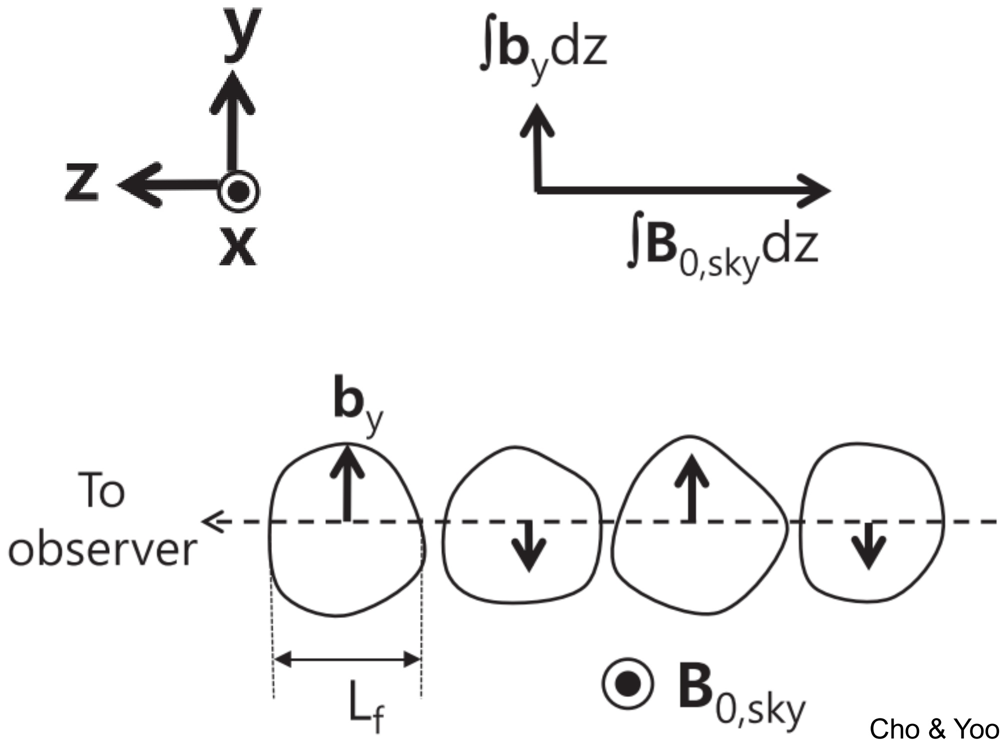

Cho & Yoo 2016

- If the driving scale is shorter than the characteristic length-scale of the cloud, multiple independent eddies exist along the LOS

- In such a case, each eddy contributes randomly to the observed turbulent field perp. to the mean field along the LOS

$$B_{\mathrm{x,obs}} \propto \int^{L_{\mathrm{los}}} (B_x + b_x)dz \sim B_{0,\mathrm{pos}} L_{\mathrm{los}}$$

- However, there is no effect on the observed field along the mean field

$$B_{\mathrm{y,obs}} \propto \int^{L_{\mathrm{los}}} b_y dz \sim b_y L_f \sqrt{L_{\mathrm{los}}/L_f}$$

$$\delta\phi \sim \frac{B_{\mathrm{y,obs}}}{B_{\mathrm{x,obs}}} \sim \frac{\delta \mathrm{b_y}}{B_{0,\mathrm{pos}}} \sqrt{L_f/L_{\mathrm{los}}} \sim \frac{\delta \mathrm{b}_{\perp,\mathrm{pos}}}{B_{0,\mathrm{pos}}} \sqrt{L_f/L_{\mathrm{los}}}$$

Extra slides

The modified DCF method (Cho & Yoo 2016)

The primary aim of the modified DCF method is to remove the averaging effects

- To get an accurate estimate of the mean field strength, a correction of the the factor of $\sqrt{L_{\rm los}/L_f}$ must be applied.
- The dispersion of LOS velocities normalized by the dispersion of the velocity centroids give a good measure of this factor i.e

$$\frac{\delta v_{\rm los}}{\delta V_c} \sim \sqrt{N} \sim \sqrt{L_{\rm los}/L_f}$$

- Thus, we can replace $\delta v_{\rm los}$ by δV_c in the DCF equation to get the modified DCF method

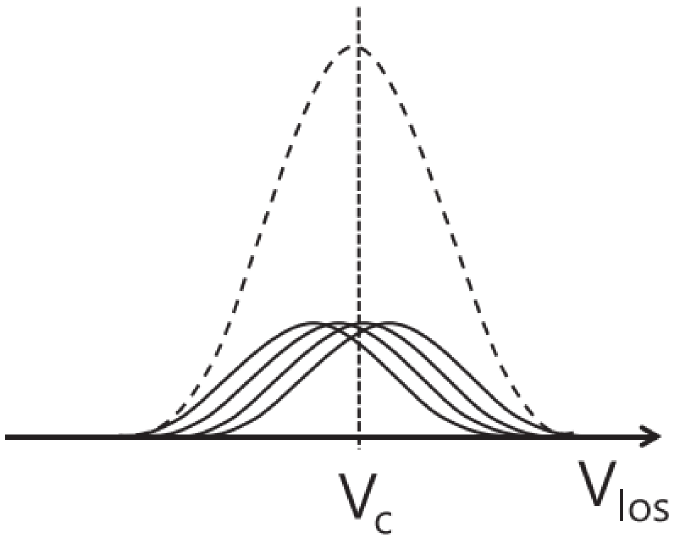

Cho & Yoo 2016

$$B_{0,\rm pos} = \xi' \sqrt{4\pi\bar{\rho}} \frac{\delta V_c}{\delta \phi}$$

with ξ' = 0.7 - 1

Extra slides

The primitive Van Vleck filter and dependence on radiation direction

- We see that the VV degeneracy becomes more apparent as the angle between radiation field and LOS decreases from 90°
- A simple filter was applied to the observed synthetic polarization maps to account for the VV flipping errors.

$$p_F = \frac{\theta_{ij} - \bar{\theta}_n}{\sigma_n}$$

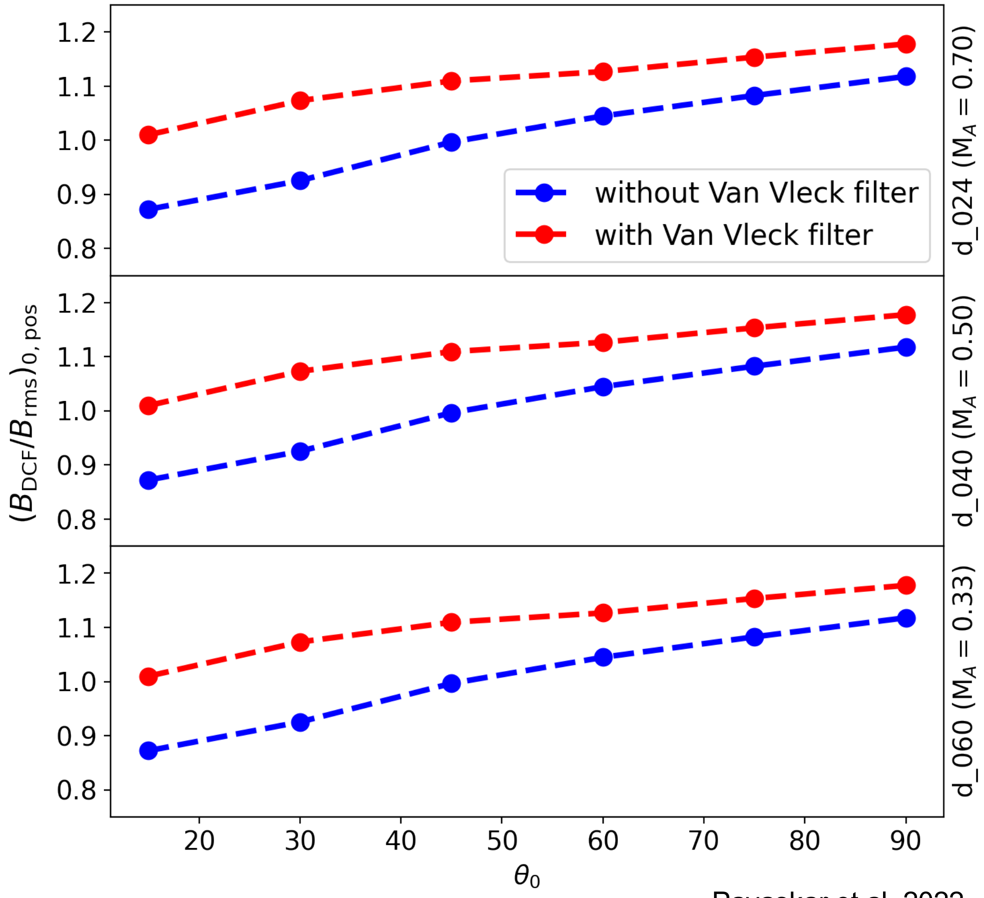

Pavaskar et al. 2022